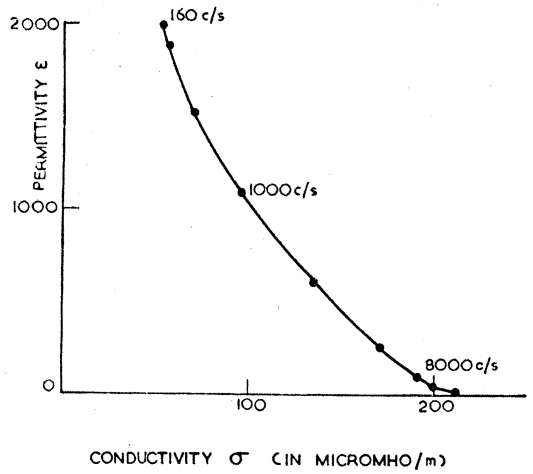

FIG. 1. Replot of Koops' data from Table I.

The loss tangent for the model is given by

$$\tan\delta \equiv \frac{4\pi\sigma}{\omega\epsilon} = \frac{4\pi}{\omega}\,\frac{\sigma_0+\omega^2\tau^2\sigma_\infty}{\epsilon_0+\omega^2\tau^2\epsilon_\infty}.$$

For the materials under discussion, $\epsilon_0/\epsilon_\infty \gg \sigma_0/\sigma_\infty$, and $\tan\delta$ then has minimum and maximum values of

$$\tan\delta_{\min} = 2(\sigma_0\sigma_\infty)^{\frac{1}{2}}/(\sigma_\infty-\sigma_0) \quad \text{at} \quad \omega\tau=(\sigma_0/\sigma_\infty)^{\frac{1}{2}},$$
$$\tan\delta_{\max} = (\epsilon_0-\epsilon_\infty)/[2(\epsilon_0\epsilon_\infty)^{\frac{1}{2}}] \quad \text{at} \quad \omega\tau=(\epsilon_0/\epsilon_\infty)^{\frac{1}{2}}.$$

From Koops' data $\sigma_\infty/\sigma_0 \approx 4$, whence $\tan\delta_{\min}=1.3$ and $\epsilon_0/\epsilon_\infty \approx 130$ giving $\tan\delta_{\max}=5.7$; these values lie close to the experimental ones of 1.4 and 6.7.

[1] C. G. Koops, Phys. Rev. **83**, 121 (1951).

The Inelastic Scattering of Fast Neutrons from Iron*

P. H. STELSON AND W. M. PRESTON
Laboratory for Nuclear Science and Engineering, Massachusetts Institute of Technology, Cambridge, Massachusetts
(Received February 13, 1952)

WITH adequate resolution and at moderate energies, the energy distribution of inelastically scattered neutrons should exhibit a "line spectrum." The theory has been given by Feld and others.[1] Experimental difficulties, particularly the low efficiency of high-resolution fast-neutron spectrometers, have thus far prevented the direct detection of separated neutron groups.

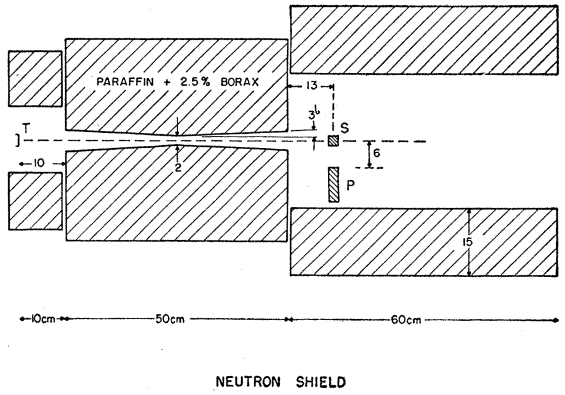

FIG. 1. Experiment arrangement for inelastic scattering of fast neutrons.

Their existence has been inferred by Feld[1] from the poor-geometry experiments of Barschall *et al.*,[2] in the case of 2–3 Mev neutrons scattered from iron, and for a number of elements by Grace *et al.*[3] by the detection of the γ-rays emitted from the low excited states in which the target nucleus is left, following inelastic scattering.

We have carried out a straightforward experiment as illustrated in Fig. 1. The neutron source, at T, was an evaporated layer of lithium having roughly 100-kev stopping power for protons at the bombarding energy of 3.61 Mev. The neutron energy distribution was, therefore, fairly uniform, from 1.82 to 1.92 Mev. The neutron beam passed through a tapered hole in the paraffin shield to the scatterer S, a cylinder of iron 2 cm in diameter and 2 cm long. Scattered neutrons were detected by the tracks of recoil protons in Eastman NTB emulsions of 200 micron thickness. The plates were placed at P, at right angles to the beam. The acceptance angle for tracks was ± 12 degrees. Exposures were for about 40 μa-hours, at an average proton current of 5 μa, but the actual monitoring was done with a BF_3 "long counter." Additional shields around the target and the plates served to reduce background from the walls of the room.

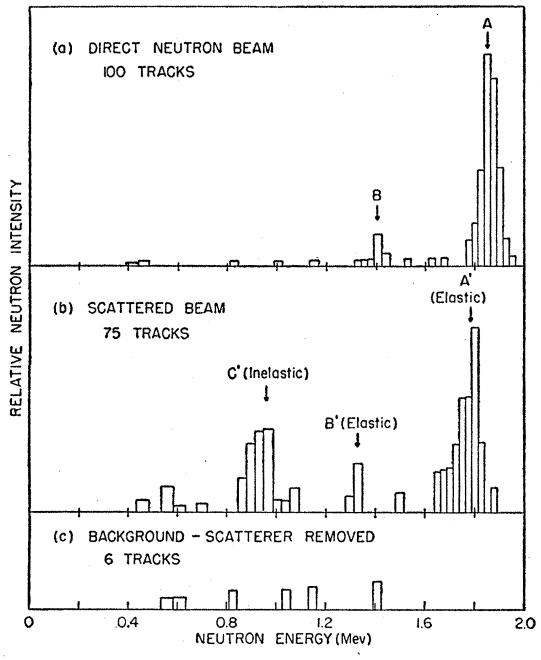

FIG. 2. Histograms of relative neutron intensity *vs* neutron energy derived from recoil proton track length distributions in nuclear track plates.

The results are shown in Fig. 2. Histogram (a) is the energy spectrum of the incident neutron beam determined by exposing plates at the position of the scatterer, S. Peaks A and B are the familiar primary and secondary neutron groups from the Li(p, n) reaction. The intensity of neutrons other than those in peaks A and B is low, showing that the arrangement produces a reasonably monoenergetic neutron beam at the position of the scatterer.

Histogram (b) is the neutron energy spectrum obtained by exposing plates at position P with the scatterer in place. Histogram (c) is the result of a similar exposure but with the scatterer removed to obtain a background measurement. The two histograms are normalized with respect to exposure time and area of emulsion measured. Corrections were applied to convert the track length distributions to relative neutron intensities.[4]

A new group of neutrons, C', is observed in the scattered neutrons shown in (b). Therefore, in addition to the elastic scattering shown by peaks A' and B', there is considerable inelastic scattering

of the primary group A to the lower energy of group C'. Neutrons of 1.87 Mev elastically scattered through 90° by iron nuclei lose 65 kev. Peak A' is ~90 kev below peak A. The somewhat larger shift is probably the result of the finite angle subtended by the scatterer at the position of the plates.

The energy of group C' indicates that a level at 850±50 kev is being excited by inelastic neutron scattering. This agrees with the result of Grace *et al.*[3] on the gamma-ray measurements. The decay schemes of Mn^{56} and Co^{56} both indicate a level at 845 kev in Fe^{56},[5] the principal iron isotope (91.5 percent). The ratio of the differential cross section for inelastic scattering to the 850-kev level, $d\sigma_{in}/d\Omega$, to the elastic scattering, $d\sigma_e/d\Omega$, at 90° for neutrons of energy 1.82 to 1.92 Mev is 0.55±0.15, as determined from the ratio of the intensity of the peak C' to A'. The consideration of track densities and exposure times for the histograms (a) and (b) gives the values $d\sigma_e/d\Omega=0.112\pm0.023$ and $d\sigma_{in}/d\Omega=0.062\pm0.015$ barn/steradian at 90° in the laboratory system. The errors indicated are the statistical errors only. The assumption of isotropic scattering gives 1.40 and 0.82 barns for σ_e and σ_{in}.

The measured total cross section of iron is about 2.8 barns at this energy, of which a large fraction should be "potential scattering" concentrated largely in the forward direction. In consequence, our rather rough determinations of absolute differential cross sections seem high. This could be the result of systematic errors.

It appears that by this method it is practical to measure elastic and inelastic differential scattering cross sections as a function of angle and incident neutron energy, with fair accuracy and resolution adequate to separate many low-lying levels in intermediate weight nuclei. It is a tedious method because of the low track densities involved, although the neutron exposure can be increased readily by a factor of ten over that used in this experiment.

We would like to thank Mrs. Gertrude Lurie for her assistance.

* This work was jointly supported by the Bureau of Ships and the ONR.

[1] B. T. Feld, Phys. Rev. **72**, 881 (1947); also AEC Technical Report NYO-636, Jan. 31, 1951.
[2] Barschall, Battat, Bright, Graves, Jorgensen, and Manley, Phys. Rev. **72**, 881 (1947).
[3] Grace, Beghian, Preston, and Halban, Phys. Rev. **82**, 969 (1951).
[4] P. H. Stelson and W. M. Preston, Phys. Rev. **82**, 655 (1951).
[5] L. G. Elliott and M. Deutsch, Phys. Rev. **63**, 321 (1943).

Domain Patterns on FeSi Crystals*

C. F. Ying, S. Levy, and R. Truell
Metals Research Laboratory, Brown University, Providence, Rhode Island
(Received January 23, 1952)

In the course of our present investigation of the effect of magnetic history on the domain patterns of 3.8 percent Si Fe-Si crystals, several interesting patterns have been observed. The sample, approximately 2.0 cm×1.5 cm×0.5 cm was grown from the melt and oriented so that its surfaces are parallel to the crystallographic planes. The domain patterns were observed by the concentrated colloid technique[1] which forms striations normal to the flux direction. These patterns reveal relatively large domains some of which have a structure. The "subdomains," whose basic pattern is of the same type as that of the main domains, can be thought of as lying within a large domain and oriented normal to it, giving rise to two types of patterns. The first pattern occurs when the fluxes in the larger domains adjacent to the substructure are parallel, Fig. 1, and the second when the fluxes in these regions are antiparallel, Fig. 2. These are easily distinguished by their respective alternating or opposing domains of closure. An explanation of Fig. 1 is given in Fig. 3 where the flux is indicated by the arrows. A similar explanation applies to Fig. 2. Long irregular chains of much smaller domains of the types shown in Figs. 1 and 2 have also been recorded. These chains were previously observed

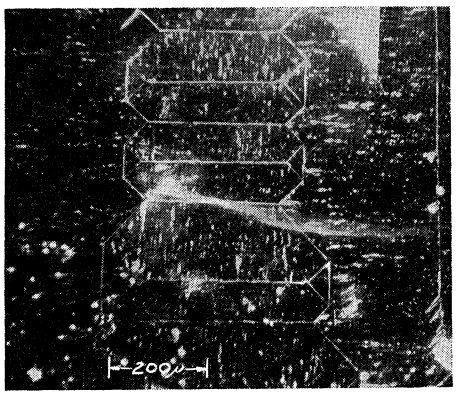

FIG. 2. Subdomain structure, type II.

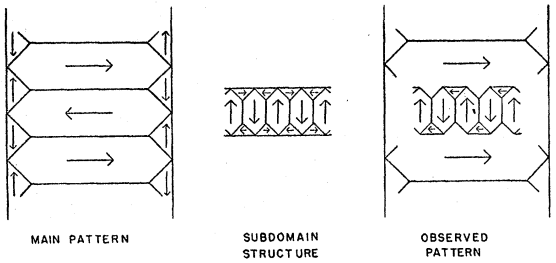

FIG. 3. Explanation of the structure of Fig. 1.

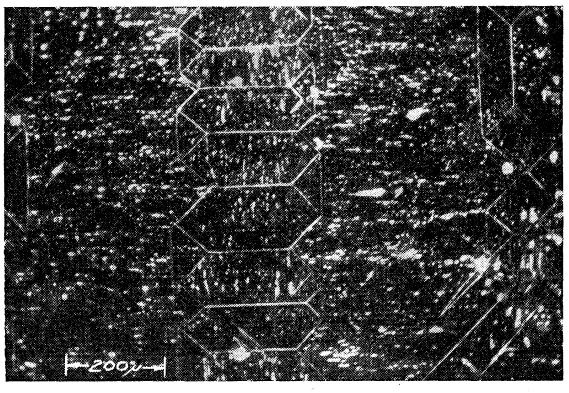

FIG. 1. Subdomain structure, type I.

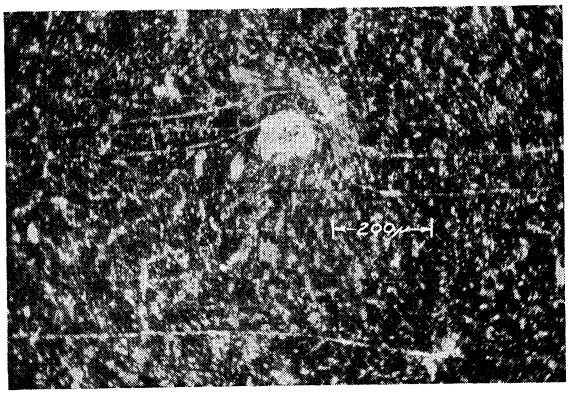

FIG. 4. Bending of a domain about an inclusion.